A 110-GHz Large-Signal Lookup-Table Model for InP HEMTs Including Impact Ionization Effects

Andrea Orzati, *Student Member, IEEE*, Dominique M. M.-P. Schreurs, *Senior Member, IEEE*, Luca Pergola, *Student Member, IEEE*, Hansruedi Benedickter, *Member, IEEE*, Franck Robin, *Student Member, IEEE*, Otte J. Homan, *Member, IEEE*, and Werner Bächtold, *Fellow, IEEE*

***Abstract*—We developed an efficient method to extract a large-signal lookup table model for InP high electron-mobility transistors that takes impact ionization into account. By measuring the device on a logarithmic frequency scale, we obtain high resolution at lower frequencies to accurately characterize impact ionization, and a sufficient number of data points at millimeter-wave frequencies to extract the nonquasi-static parameters. Model validation through linear and nonlinear device measurements and its application to monolithic-microwave integrated-circuit design are presented.**

***Index Terms*—Impact ionization, InP high electron-mobility transistors (HEMTs), large-signal model.**

I. Introduction

InP HIGH electron-mobility transistors (HEMTs) are widely used for millimeter-wave applications because their performance is better than that of GaAs-based MESFETs and HEMTs in terms of both gain and noise figure. For this reason, it is important to carefully model the linear and nonlinear characteristics of these devices in the millimeter-wave frequency range. However, an InP HEMT large-signal model should also describe the device behavior in the lower gigahertz range in order to allow accurate simulation of frequency-shifting circuits such as mixers or frequency multipliers. One of the most important effects in this frequency range is the so-called kink effect related to impact ionization [1]. Due to the smaller bandgap of the InGaAs channel, impact ionization in InP HEMTs occurs at drain–source voltages, which are lower than in GaAs-based devices, and results in high gate leakage current, high output conductance, and low breakdown voltage. Impact ionization effects can be observed at operating conditions that are typical for nonlinear circuits and should, therefore, be taken into account by large-signal models. Works on FET device modeling have already been reported, but they are either limited to verification at microwave frequencies [2], [3], to a bias-dependent small-signal model [4], [5], or to GaAs FETs [6], where impact ionization is normally not considered. In this paper, we present a large-signal lookup-table-based model for InP HEMTs, which has been verified up to millimeter-wave frequencies and takes impact ionization into account. Since the model is mainly addressing the design of low-power amplifiers and frequency-shifting circuits, power-related effects such as self-heating can be neglected. In the following sections, we introduce the used small- and large-signal topologies, the modeling procedure, and its validation through device nonlinear measurements. Finally, we present the application of the model to the design of linear and nonlinear circuits in a frequency range from 16 to 64 GHz.

Manuscript received November 19, 2002; revised July 8, 2002. This work was supported by the Swiss Commission for Technology and Innovation.

A. Orzati, L. Pergola, H. Benedikter, F. Robin, O. J. Homan, and W. Bächtold are with the Laboratory for Electromagnetic Fields and Microwave Electronics, Eidgenössische Technische Hochschule, CH-8092 Zürich, Switzerland.

D. M. M.-P. Schreurs is with the Electronics, Systems, Automation, and Technology Department, Telecommunications and Microwaves Division, Katholieke Universiteit Leuven, 10, B-3001 Leuven, Belgium.

Digital Object Identifier 10.1109/TMTT.2002.807823

II. Equivalent Circuit

The devices we used for the model extraction are two-finger InP HEMTs with 0.2-μm gate length, 75-μm gate-finger width, 135-GHz f_T, and 200-GHz $f_{\max}$ fabricated using our in-house process. The modeling procedure is an extension of the method presented and used for GaAs pseudomorphic high electron-mobility transistors (pHEMTs). In [7], where only experimental results up to microwave frequencies are shown, a nonquasi-static small-signal model and its corresponding large-signal model are presented, where the feedback elements between the gate and drain terminals are eliminated and replaced with transelements. For millimeter-wave effects and impact ionization to be included into the model, some modifications have to be made both to the small- and large-signal equivalent schemes. At millimeter-wave frequencies, the electrical length of gate and drain metallizations becomes relevant and transmission-line effects need to be included. This is achieved by splitting the extrinsic gate and drain capacitances in two [4], [5]. Since we are considering bias-independent extrinsic elements, this splitting does not influence the large-signal equivalent scheme.

In order to model impact ionization effects, we add an extra network at the drain side of the small-signal equivalent circuit [8]. This network consists of a resistance R_{im} in series with the parallel connection of a capacitance C_{im} and a transconductance g_{im} controlled by the intrinsic drain–gate voltage V_{dgi}. The small-signal equivalent circuit and the intrinsic large-signal equivalent circuit are showed in Figs. 1 and 2, respectively.

The large-signal representation of the transistor consists of the parallel connection of a charge and current source at the drain side and of a current source in parallel with the series connection of a charge source and a resistor at the gate side. This large-signal equivalent circuit is consistent with the intrinsic small-signal equivalent scheme already introduced. It is important to find a large-signal representation of the impact ionization network. Based on our experimental results, we found

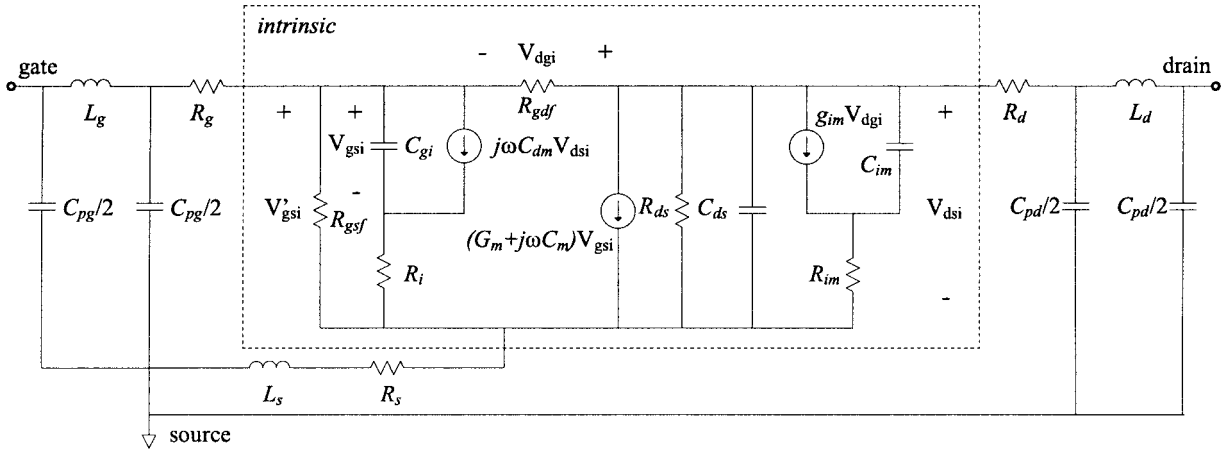

Fig. 1. Small-signal equivalent scheme.

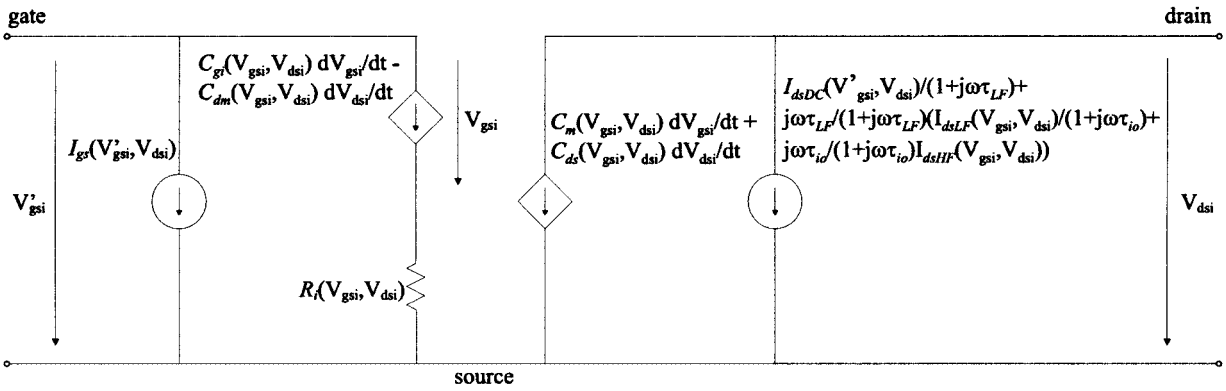

Fig. 2. Large-signal equivalent scheme.

out that it can be best treated as a first-order dispersive network. It is similar to the modeling approach of the dispersive behavior of G_m and $G_{\rm ds}$ in the kilohertz–megahertz range [9]. The bias-dependent values of G_m and $G_{\rm ds}$ are extracted twice, once at frequencies lower than those of interest for impact ionization (250 MHz–0.5 GHz), the second time at frequencies where impact ionization does not influence the S-parameters anymore (7–110 GHz). It must be noticed that, in our case, at 250 MHz, which is the lowest measurement frequency, the low-frequency output dispersion is not effective anymore. From the integration of G_m and $G_{\rm ds}$ toward their intrinsic terminal voltages, we obtain the low-frequency drain–source current $I_{\rm dsLF}$ and the high-frequency drain current $I_{\rm dsHF}$. Another point worth noticing is that the capacitances are not integrated, but are directly used as bias dependent, as already successfully reported in [10] and [11]. At the gate side, this is mathematically equivalent since charge conservation is guaranteed, nevertheless one should be aware of possible peculiarities. The average capacitive current might not be zero, leading to nonconservation of energy [12]. At the drain side, charge conservation is not necessarily guaranteed since two capacitances with two different physical meanings are used; $C_{\rm ds}$ is a space-charge capacitance and C_m is related to the intrinsic time delay τ. The large-signal equivalent circuit is complete after adding another first-order transfer function, which regulates the transition between the measured dc current $I_{\rm dsDC}$ and the low-frequency current $I_{\rm dsLF}$ [9], thus modeling the low-frequency output dispersion.

III. Model Extraction

The first step of the modeling procedure is the extraction of the bias-independent extrinsic parameters. This is done from cold ($V_{\rm ds} = 0$) measurements using the method described in [13]. The advantage of this method is that the gate–current density is kept much lower than in other similar methods used for MESFETs, thus avoiding a possible device degradation.

Then, the device S-parameters are measured over a grid of over 900 different bias points. Here, it is worth pointing out that, in a lookup-table-based large-signal model, the capability of predicting high-order harmonics is limited by the precision of the interpolation between the points where the model is actually defined. Since the most important nonlinearity is due to the drain–source current, we decided to use variable steps for $V_{\rm gs}$ and $V_{\rm ds}$ and have a tighter grid where the drain–source current changes more drastically, i.e., close to the threshold voltage for $V_{\rm gs}$ and in the linear region for $V_{\rm ds}$.

In order to obtain a good accuracy up to millimeter-wave frequencies, it is not enough to measure the S-parameters at only one frequency point. In this case, it would be also impossible to have any information about the impact ionization effects,

which are strongly frequency dependent. On the other hand, in order to achieve a sufficient resolution in the low-frequency range using a linear sweep, at least 201 frequency points would be necessary, thus generating a huge amount of data, not to mention the long time required by the measurements. What is needed is a good resolution at low frequencies to extract the impact-ionization-related parameters, and only few points in the millimeter-wave frequency range, which are sufficient to extract the other parameters. Therefore, we chose to use a logarithmic frequency sweep that reaches the goal using only 59 points. This is important because it improves the measurement speed and drastically reduces the computation time. The intrinsic small-signal elements are calculated according to the following expressions:

$$G_{\rm ds} = \Re(Y_{22}) \tag{1}$$

$$G_m = \Re(Y_{21} - Y_{12}) \tag{2}$$

$$R_i = \Re\big(1/(Y_{11} - Y_{11\rm DC})\big) \tag{3}$$

$$C_{gi} = -1/\big(2\pi f \Im(1/Y_{11})\big) \tag{4}$$

$$C_{dm} = C_{gi}\left|\frac{Y_{12}}{Y_{11}}\right| \tag{5}$$

$$C_{\rm ds} = -1/\big(2\pi f \Im(1/Y_{22})\big) \tag{6}$$

$$C_m = \Im(Y_{21} - Y_{12})/(2\pi f) \tag{7}$$

$$\tau_{io} = \frac{1}{f|_{\min(Y_{22})}}. \tag{8}$$

In (3), $Y_{11\rm DC}$ is subtracted from Y_{11} because the $I_{\rm gs}$ state function is directly measured at dc. This is allowed by the nondispersive behavior of $I_{\rm gs}$. The values of $G_{\rm ds}$ and G_m leading to $I_{\rm dsLF}$ are extracted at the lowest measurable frequency (250 MHz). $G_{\rm ds}$ used in $I_{\rm dsHF}$ is extracted at a frequency equal to $1/\tau_{io}$. G_m used in $I_{\rm dsHF}$ and all the other intrinsic component can be well determined by taking their mean value over the 10–25-GHz range, where no dispersive effect takes place. All the measurements and extraction of the small-signal parameters are performed using HP IC-CAP. A possible degradation of the device due to the multibias S-parameter measurements is checked by comparison of the dc and RF characteristics before and after the measurement process [14]. This is done to ensure the validity of the extraction procedure. After the small-signal parameter extraction, integration is performed using numerical routines implemented in MATLAB. For the model to be handled in a nonlinear circuit simulator as HP ADS, the intrinsic terminal voltages $V_{\rm gsi}$ and $V_{\rm dsi}$ contained in the lookup tables must lie on an orthogonal grid. At the same time, the extrinsic terminal voltages $V_{\rm gse}$ and $V_{\rm dse}$ need to also be on an orthogonal grid, otherwise one would have to define one by one all the different bias points used in device measurements. The intrinsic and the extrinsic terminal voltages are related by the following equations:

$$V_{\rm dsi} = V_{\rm dse} - (R_{\rm dc2} + R_{\rm d} + R_{\rm s})I_{\rm ds}(V_{\rm gse}, V_{\rm dse}) - R_{\rm s}I_{\rm gs}(V_{\rm dse}, V_{\rm gse}) \tag{9}$$

$$V_{\rm gsi} = V_{\rm gse} - (R_{\rm dc1} + R_{\rm g} + R_{\rm s})I_{\rm gs}(V_{\rm gse}, V_{\rm dse}) - R_{\rm s}I_{\rm ds}(V_{\rm dse}, V_{\rm gse}). \tag{10}$$

In (9) and (10) $R_{\rm dc1}$ and $R_{\rm dc2}$ are the resistances of the cables used to bias the device and $R_{\rm g}$, $R_{\rm d}$, and $R_{\rm s}$ are the extrinsic gate, drain, and source resistance, respectively. From (9) and (10), it is clear that measuring using an orthogonal extrinsic-voltages grid does not lead to an orthogonal intrinsic-voltages grid. We solve the problem by generating an orthogonal intrinsic-voltages grid and interpolating the values of the small-signal intrinsic parameters expressed as a function of the nonorthogonal intrinsic voltages on the orthogonal intrinsic-voltages grid. In this way, we can integrate the small-signal intrinsic parameters on an orthogonal grid. As it shown in Section IV, this interpolation does not affect the precision of the model.

After performing the numerical integration and generating the lookup tables as CITI files, the model is implemented in HP ADS as a symbolically-defined device.

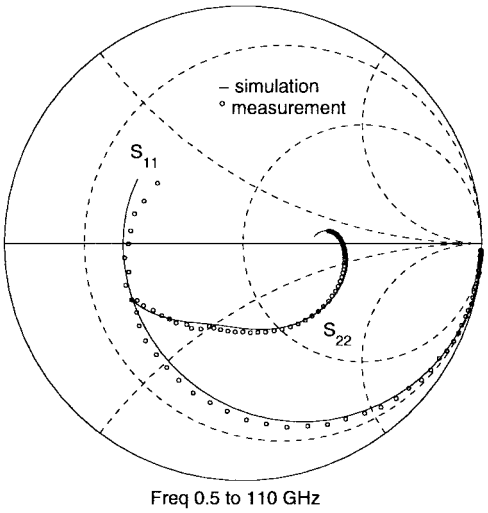

Fig. 3. Comparison between measured (symbols) and simulated (solid line) S-parameters at $(V_{\rm gs},\ V_{\rm ds}) = (-0.2\ \text{V},\ 1.4\ \text{V})$.

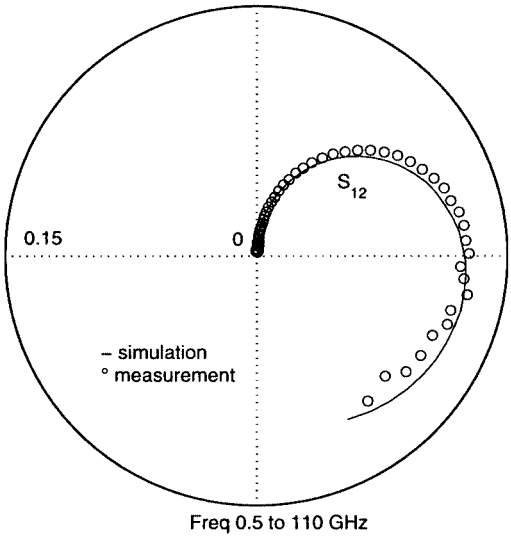

Fig. 4. Comparison between measured (symbols) and simulated (solid line) S-parameters at $(V_{\rm gs},\ V_{\rm ds}) = (-0.2\ \text{V},\ 1.4\ \text{V})$.

IV. Small- and Large-Signal Model Validation

The accuracy and limitations of the model were tested under both small- and large-signal conditions. Figs. 3–6 report measured and simulated S-parameters at a bias point ($V_{\rm gs} = -0.2$ V,

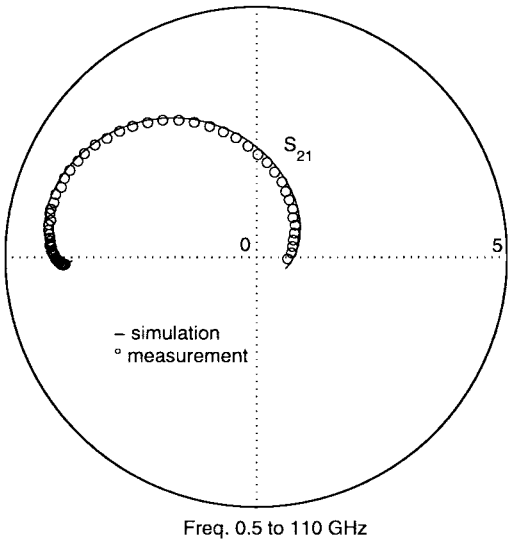

Fig. 5. Comparison between measured (symbols) and simulated (solid line) S-parameters at $(V_{\rm gs},\ V_{\rm ds}) = (-0.2\ \text{V},\ 1.4\ \text{V})$.

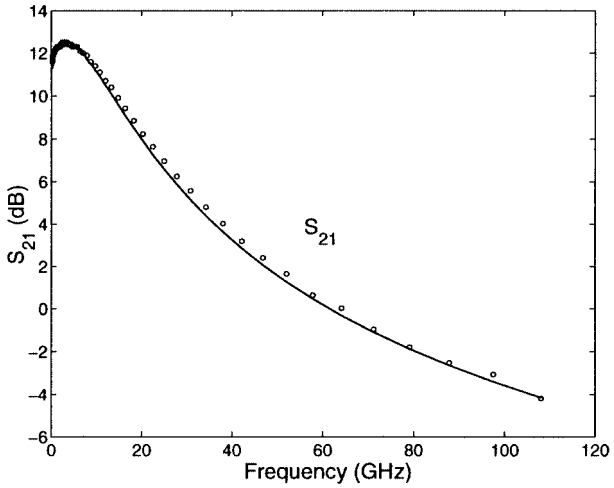

Fig. 6. Comparison between measured (symbols) and simulated (solid line) S-parameters at $(V_{\rm gs},\ V_{\rm ds}) = (-0.2\ \text{V},\ 1.4\ \text{V})$.

$V_{\rm ds} = 1.4$ V) where impact ionization is already taking place, as can be seen from the inductive behavior of S_{22} and the reduced value of S_{21} at low frequencies. In order to better visualize the effect of impact ionization, the power gain S_{21} is shown both on a polar plot and on a decibel scale (Figs. 5 and 6). The good agreement between measurements and simulations from the lower gigahertz range up to 110 GHz validates the small-signal modeling approach and confirms that a first-order transfer function effectively models the transition between the low-frequency drain current $I_{\rm dsLF}$ and the high-frequency drain current $I_{\rm dsHF}$. After the small-signal verification, the model was tested under nonlinear operating conditions. In Fig. 7, a comparison between measured and simulated third-order intermodulation is shown. The measurements were performed in a frequency region (3.5 GHz) and at bias point ($V_{\rm gs} = -0.2$ V, $V_{\rm ds} = 1.4$ V) where impact ionization is affecting the device. The model predicts very well the output power of the fundamental tone, as well as of the intermodulation product. This attests that the used model can successfully reproduce the large-signal effects of im-

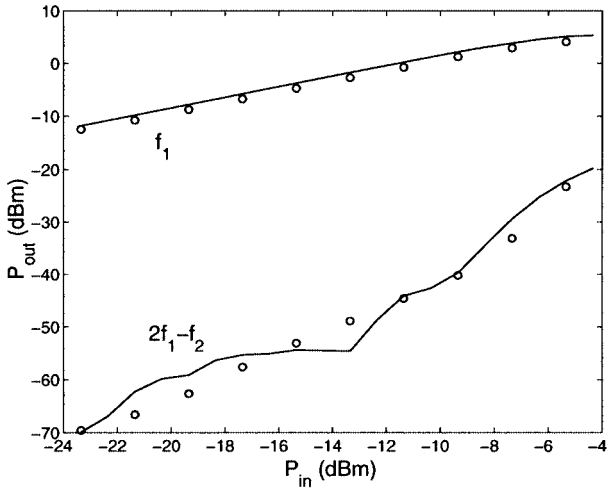

Fig. 7. Comparison between measured (symbols) and simulated (solid line) third-order intermodulation. $f_1 = 3.5$ GHz, $f_2 = 3.501$ GHz. $P_{\rm in}$ represents the power of a single tone. The dc-bias point is $(V_{\rm gs},\ V_{\rm ds}) = (-0.2\ \text{V},\ 1.4\ \text{V})$.

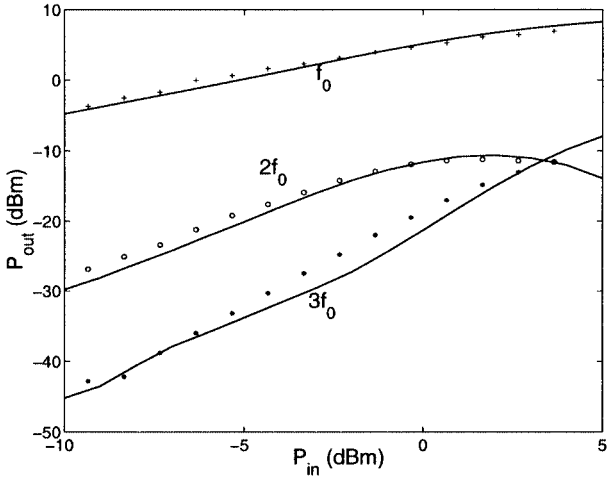

Fig. 8. Measurements (symbols) and simulated (solid line) output power versus input power at the fundamental frequency of 16 GHz and the corresponding second and third harmonics. The dc-bias point is $(V_{\rm gs},\ V_{\rm ds}) = (-0.3\ \text{V},\ 1\ \text{V})$.

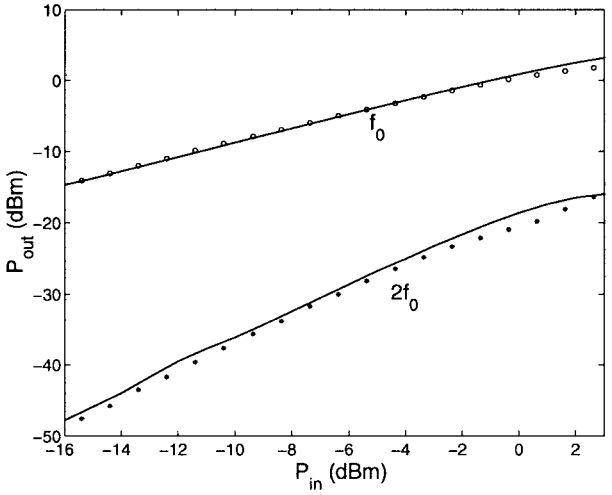

Fig. 9. Measurements (symbols) and simulated (solid line) output power versus input power at the fundamental frequency of 32 GHz and the corresponding second harmonic. The dc-bias point is $(V_{\rm gs},\ V_{\rm ds}) = (-0.3\ \text{V},\ 0.7\ \text{V})$.

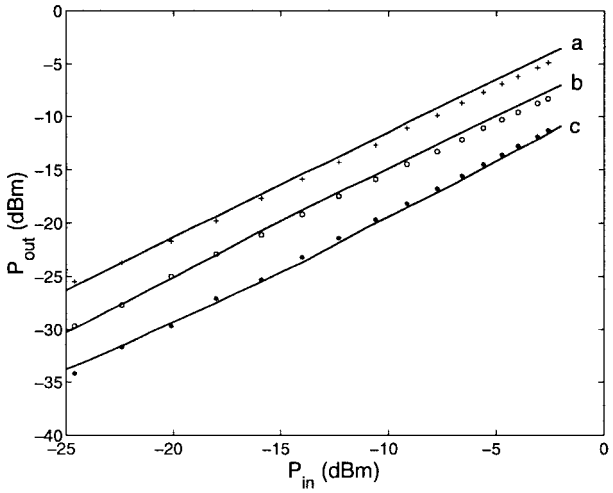

Fig. 10. Measured (symbols) and simulated (solid line) output power versus input power at 64 GHz at three different bias points: $(V_{\rm gs}, V_{\rm ds})$ = (a) $(-0.2$ V, 1 V), (b) $(-0.4$ V, 1 V), (c) $(-0.4$ V, 0.5 V).

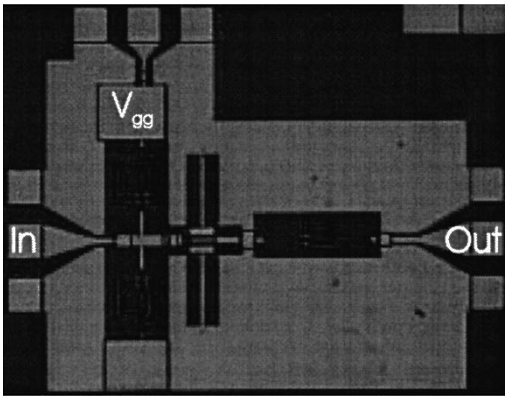

Fig. 11. Photograph of the 16-GHz amplifier. Circuit size is 1.4×1 mm^2.

pact ionization. Fig. 8 shows the measured and simulated harmonics at a fundamental frequency of 16 GHz. As we can see, the prediction capability of the model is accurate up to the third harmonic. This is a clear indication that the interpolation method used to generate the lookup tables is suitable. Fig. 9 shows the measured and simulated harmonics at a fundamental frequency of 32 GHz. In Fig. 10, the measured and simulated output power at a fundamental frequency of 64 GHz is shown for three different dc-bias points. The first bias point, i.e., (a), corresponds to class-A operation. In the second, i.e., (b), $V_{\rm gs}$ is close to V_T and $V_{\rm ds}$ is in the saturation region. In the third, i.e., (c), $V_{\rm gs}$ is close to V_T and $V_{\rm ds}$ is in the linear region.

V. Application to MMIC Design

The large-signal model discussed in the previous sections was used to design various circuits. In this section, we describe the comparison between measurements and simulations for a 16-GHz amplifier, a 64-GHz amplifier, and a 62-GHz active mixer. Photographs of these circuits are shown in Figs. 11–13, respectively. The mixer is an up-converting mixer that uses a 48-GHz local oscillator (LO) to convert a signal in the 14–15-GHz band up to 62–63 GHz. The LO and IF are both applied at the same port using an external diplexer. Measured

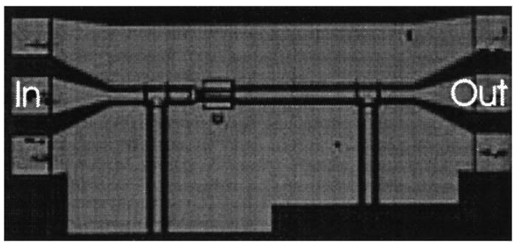

Fig. 12. Photograph of the 64-GHz amplifier. Circuit size is 1.2×0.54 mm^2. The circuit is biased through external bias tees.

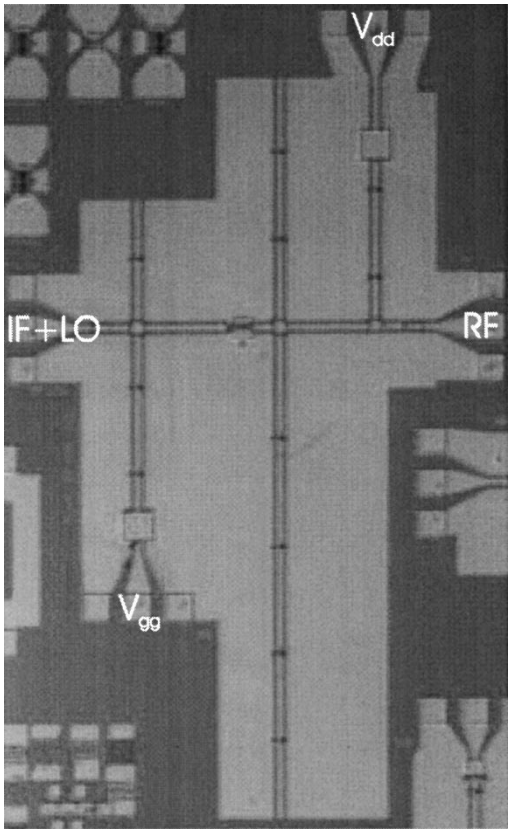

Fig. 13. Photograph of the 62-GHz up-converting active mixer. Circuit size is 1.6×3 mm^2.

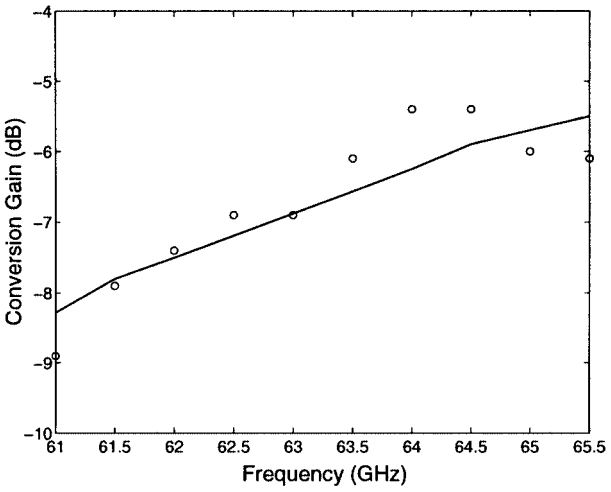

Fig. 14. Measured (symbols) and simulated (solid line) conversion gain of the 62-GHz active mixer.

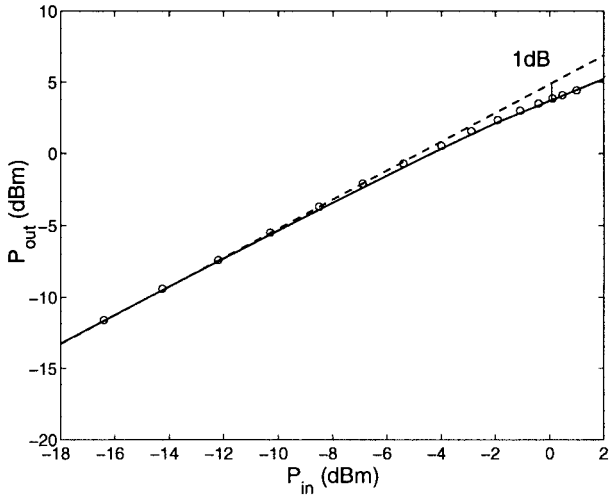

Fig. 15. Measured (symbols) and simulated (solid line) 1-dB compression point of the 64-GHz amplifier.

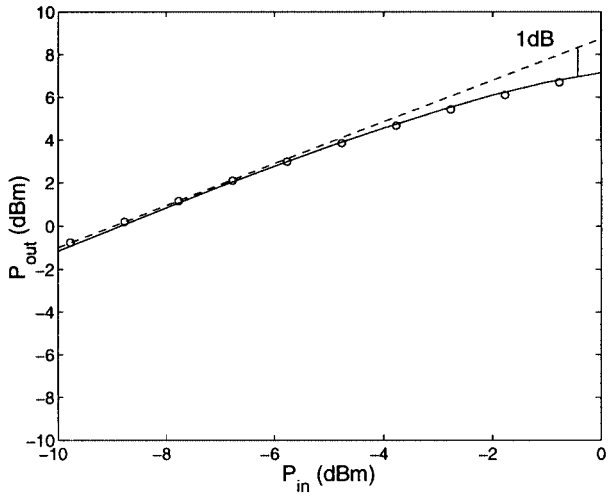

Fig. 16. Measured (symbols) and simulated (solid line) 1-dB compression point of the 16-GHz amplifier.

and simulated conversion gain as a function of frequency for an LO power of −5 dBm, which was the highest available power, and an IF power of −15 dBm are shown in Fig. 14. Figs. 15 and 16 report the measured and simulated 1-dB compression points for the 64- and 16-GHz amplifiers, respectively. The good agreement of measurements and simulations confirms the validity of our modeling approach.

VI. Conclusions

In this paper, we have described an efficient procedure to extract a lookup-table-based InP HEMTs large-signal model, which takes impact ionization effects into account. Using a logarithmic frequency sweep, we significantly reduce measurement and extraction times. With S-parameter measurements, we demonstrate that the linear performance of the model is excellent up to 110 GHz. The nonlinear performance is validated up to 64 GHz by nonlinear measurements. It is also demonstrated that our large-signal model can be successfully used to predict the performances of amplifiers and mixers in the 60-GHz band.

References

[1] M. H. Somerville, J. A. del Alamo, and W. Hoke, "Direct correlation between impact ionization and the kink effect in InAlAs/InGaAs HEMTs," *IEEE Electron Device Lett.*, vol. 17, pp. 473–475, Oct. 1996.

[2] D. E. Root, S. Fan, and J. Meyer, "Technology independent large signal non quasistatic FET models by direct construction from automatically characterized device data," in *Proc. 21th Eur. Microwave Conf.*, 1991, pp. 927–932.

[3] C. J. Wei, Y. A. Tkachenko, and D. Bartle, "Table-based dynamic FET model assembled from small-signal models," *IEEE Trans. Microwave Theory Tech.*, vol. 47, pp. 700–705, June 1999.

[4] P. J. Tasker and J. Braunstein, "New MODFET small-signal circuit model required for millimeter-wave MMIC design: Extraction and validation to 120 GHz," in *IEEE MTT-S Int. Microwave Symp. Dig.*, 1995, pp. 611–614.

[5] J. Wood and D. Root, "Bias-dependent linear, scalable millimeter-wave FET model," in *IEEE MTT-S Int. Microwave Symp. Dig.*, 2000, pp. 1381–1384.

[6] M. Fernandez-Barciela, P. J. Tasker, Y. Campos-Roca, M. Demmler, H. Massler, E. Sanchez, M. C. Curras-Francos, and M. Schlechtweg, "A simplified broad-band large-signal nonquasi-static table-based FET model," *IEEE Trans. Microwave Theory Tech.*, vol. 48, pp. 395–405, Mar. 2000.

[7] P. Jansen, D. Schreurs, W. De Raedt, B. Nauwelaers, and M. Van Rossum, "Consistent small-signal and large-signal extractions techniques for heterojunction FET," *IEEE Trans. Microwave Theory Tech.*, vol. 43, pp. 87–93, Jan. 1995.

[8] R. Reuter, M. Agethen, U. Auer, S. van Waasen, D. Peters, W. Brockerhoff, and F. J. Tegude, "Investigation and modeling of impact ionization with regard to the RF and noise behavior of HFET," in *IEEE MTT-S Int. Microwave Symp. Dig.*, 1997, pp. 1317–1320.

[9] D. Root, "Analysis and exact solutions of relaxation-time differential equations describing non quasistatic large signal FET models," in *Proc. 24th Eur. Microwave Conf.*, 1994, pp. 854–859.

[10] D. S. McPherson, K. Elgaid, I. G. Thayne, I. D. Robertson, and S. Lucyszyn, "Ultra-broadband nonlinear pHEMT modeling using TOPAS," in *8th IEEE Int. High-Performance Electron Devices for Microwave and Optoelectronic Applications Symp.*, 2000, pp. 85–88.

[11] C. J. Wei, Y. A. Tkachenko, J. Gering, and D. Bartle, "Completely consistent "no-charge" pHEMT model including DC/RF dispersion," in *IEEE MTT-S Int. Microwave Symp. Dig.*, 2002, pp. 2133–2136.

[12] D. Root, "Elements of measurements-based large-signal device modeling," in *Proc. RAWCON Modeling and Simulation of Devices and Circuits for Wireless Communication Systems Workshop*, 1998, p. 34.

[13] D. Schreurs, Y. Baeyens, B. K. J. C. Nauwelaers, W. De Raedt, M. Van Hove, and M. Van Rossum, "S-parameter measurements based quasistatic large-signal cold HEMT model for resistive mixer design," *Int. J. Microwave Millimeter-Wave Computer-Aided Eng.*, vol. 6, no. 4, pp. 250–258, 1996.

[14] D. Schreurs, A. Spiers, W. De Raedt, K. Van Der Zanden, Y. Baeyens, M. Van Hove, B. Nauwelaers, and M. Van Rossum, "DC, LF dispersion and HF characterization of short-time stressed InP based LM-HEMTs," in *Proc. 7th Eur. Reliability of Electron Devices, Failure Physics and Analysis Symp.*, 1996, pp. 1911–1914.

Andrea Orzati (S'99) was born in Cagliari, Italy, in 1973. He received the Master degree in electronic engineering from the University of Cagliari, Cagliari, Italy, in 1998, and is currently working toward the Ph.D. degree at the Eidgenössische Technische Hochschule (ETH) Zürich, Switzerland.

In October 1998 he joined the InP Technology Group, ETH. His research interests are millimeter-wave circuit design and characterization, device modeling, and packaging.

Dominique M. M.-P. Schreurs (S'90–M'97–SM'02) received the M.Sc. degree in electronic engineering and Ph.D. degree (with honors) from the Katholieke Universiteit Leuven (K.U.Leuven), Leuven, Belgium, in 1992 and 1997, respectively.

She is currently a Post-Doctoral Fellow of the Fund for Scientific Research-Vlaanderen and a Visiting Assistant Professor with the K.U.Leuven. She has been a Visiting Scientist with Agilent Technologies, the Eidgenössische Technische Hochschule (ETH), Zürich, Switzerland, and the National Institute of Standards and Technology (NIST). Her main research interest is the use of vectorial large-signal measurements for the characterization and modeling of nonlinear microwave devices.

Luca Pergola (S'01) was born in Cagliari, Italy, in 1974. He received the Master degree in electronic engineering from the University of Cagliari, Cagliari, Italy, in 2000, and is currently working toward the Ph.D. degree at the Eidgenössische Technische Hochschule (ETH), Zürich, Switzerland.

In January 2001, he joined the Electromagnetic Field Theory Group, ETH. His current research fields are, planar antennas, antenna arrays and low-temperature co-fired ceramic (LTCC) technology.

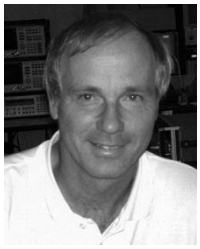

Hansruedi Benedickter (S'81–M'85) was born in on April 20, 1951, in Zug, Switzerland. He received the Diploma degree in electrical engineering from the Eidgenössische Technische Hochschule (ETH), Zürich, Switzerland, in 1976.

He has been a Research Assistant and Senior Research Associate with the Microwave Laboratory, ETH, and, since 1987, with the Laboratory for Electromagnetic Fields and Microwave Electronics. His main research interests are microwave, millimeter-wave, and on-wafer measurement techniques.

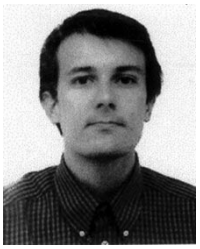

Franck Robin (S'98) received the Engineering degree in material sciences and semiconductor physics and the Master degree in integrated electronics from the National Institute for Applied Sciences (INSA) Lyon, France, in 1996 and 1999, respectively, and is currently working toward the Ph.D. degree at the Eidgenössische Technische Hochschule (ETH), Zürich, Switzerland.

From 1995 to 1997, he was with the ETH, Lausanne, Switzerland, where he was involved with low-frequency noise characterization of InP HEMTs. In 1998, he joined the InP Technology Group, ETH. His research interests include physical device and process modeling, InP HEMT technology and characterization, and the fabrication of integrated optical devices.

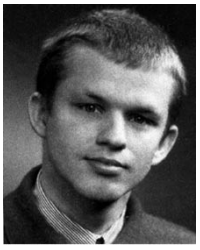

Otte J. Homan (M'98) was born in Vries, The Netherlands, in 1968. He received the Engineering degree in applied physics from the University of Groningen, Groningen, The Netherlands, in 1992, and the Ph.D. degree in technical sciences from the Eidgenössische Technische Hochschule (ETH), Zürich, Switzerland, in 1996

From 1992 to 1996 he was with the Paul Scherrer Institute, Zürich, Switzerland, where he focused on the design and manufacturing of laser diodes with side-coupled Bragg gratings. Since 1996, his main professional interest has been the design, fabrication, and applications of high-speed low-noise InP HEMT devices, circuits, and MMICs.

Werner Bächtold (M'71–SM'99–F'00) was born October 1, 1939. He received the Diploma degree and Ph.D. degree in electrical engineering from the Eidgenössische Technische Hochschule (ETH), Zürich, Switzerland, in 1964 and 1968, respectively.

From 1969 to 1987, he was with the IBM Zürich Research Laboratory, where he was involved with device and circuit design and analysis of GaAs MESFETs, design of logic and memory circuits with Josephson junctions, and semiconductor lasers for digital communication. He was on assignment with the IBM T. J. Watson Research Center, Yorktown Height, NY. Since December 1987, he has been a Professor of electrical engineering at the ETH. He heads the Microwave Electronics Group, Laboratory for Electromagnetic Fields and Microwave Electronics. He is engaged with design and characterization of MMICs, design and technology of InP-HEMT devices and circuits, as well as microwave photonics.